Xu, Jinzhao; Wang, Jun; Chen, Yuzhu; Xu, Zhicheng; Lund, Peter D.

Thermo-ecological cost optimization of a solar thermal and photovoltaic integrated energy system considering energy level

Published in:
Sustainable Production and Consumption

DOI:
10.1016/j.spc.2022.07.011

Published: 01/09/2022

Document Version
Peer-reviewed accepted author manuscript, also known as Final accepted manuscript or Post-print

Please cite the original version:
Xu, J., Wang, J., Chen, Y., Xu, Z., & Lund, P. D. (2022). Thermo-ecological cost optimization of a solar thermal and photovoltaic integrated energy system considering energy level. *Sustainable Production and Consumption*, *33*, 298-311. https://doi.org/10.1016/j.spc.2022.07.011

Thermo-ecological cost optimization of a solar thermal and photovoltaic integrated energy system considering energy level

Jinzhao Xu [a], Yuzhu Chen [a], Zhicheng Xu [a], Jun Wang [a*], Peter D. Lund [a, b]

[a] Key Laboratory of Solar Energy Science and Technology in Jiangsu Province, Southeast University, No 2 Si Pai Lou, Nanjing, 210096, China

[b] School of Science, Aalto University, P.O. Box 15100, FI-00076, Aalto (Espoo), Finland

* Corresponding authors: Jun Wang; e-mail: 101010980@seu.edu.cn;

Abstract

Integrating renewable resources into traditional tri-generation systems helps to reduce fossil fuel use and emissions. A solar thermal and photovoltaic assisted integrated energy system is proposed here using high-performance cooling approaches to provide cooling, heating and electricity. To find the best system configurations with a focus on the ecological performance, the specific thermo-ecological cost of the energy products considering energy level were optimized employing the cumulative exergy consumption over the whole life-cycle.. The results show that the ideal specific costs for cooling, heating and electricity demands are 8.70, 7.13, and 1.97 J/J, respectively. Compared to the method without the energy level consideration, the specific cost of the hybrid system is 0.47 J/J higher due to the lower energy level of water products. Moreover, the specific thermo-ecological cost of natural gas has higher impacts on the performance of hybrid system than the other parameters.

Keywords: Integrated energy system; Thermo-ecological assessment; Cumulative exergy; Equivalent pollutant emissions; Energy level; Multi-objective optimization

Abbreviations

AHP	Absorption heat pump
ASHP	Air source heat pump
GT	Gas turbine
HE	Heat exchanger

IES	Integrated energy system
LCA	Life-cycle assessment
PTC	Parabolic trough collector
PV	Photovoltaic
STP	Solar thermal and photovoltaic
WCC	Water-cooled chiller
Symbols	
A	Area, m^2
C	Capacity, kW
CEC	Compensate exergy consumption, kWh
CExE	Cumulative exergy consumption, kWh
COP	Coefficient of performance
E	Electricity, kWh
ExE	Exergy, kWh
f	Partial load, %
F	Fuel, kWh
m	Mass, kg
Q	Thermal, kWh
S	Irradiance, W/m^2
STEC	Specific thermo-ecological cost, J/J
T	Temperature, °C
V	Variable coefficient
$\bar{x}$	Normalized value
X	Index
Greek symbols	
η	Efficiency, %
κ	Temperature coefficient, 1/°C
γ	Heating ratio
ω	Weight
Superscript/ Subscript	
a	Ambient
c/h	Chilled/heating water
ch	charge
dis	Discharge
eqv	Equivalent

i/h	*i/h*th process
j	*j*th hour
k	*k*th index
min/max	Minimum/maximum
NE	Non-renewable energy
NG	Natural gas
p	Pollutant
std	Standard test condition
t	Total
tk	Tank

1 Introduction

Using local renewable energy is an effective way to reduce fossil fuel consumption and the address climate change. Among the renewable energy alternatives, solar energy is easily applied for and in buildings due to the widespread distribution of the solar radiation resource(Madathil, V, Nair, Jamasb, & Thakur, 2021). However, the low energy density and intermittent nature of solar irradiance limits its large-scale utilization. Through integration of solar energy to conventional energy systems, such as tri-generation, the use of solar energy could be enhanced, but still enabling dispatchable energy production(Kasaeian, Bellos, Shamaeizadeh, & Tzivanidis, 2020). This work also focusses on solar-assisted tri-generation by employing solar thermal (PTC) and photovoltaics (PV).

Previous work on solar-assisted tri-generation work includes that of Wang et al. (Wang, Han, & Guan, 2020) who described possible layouts for solar assisted tri-generation systems using solar collectors to generate thermal energy at specific temperatures to generate hot water, chilled water, but also to drive prime mover to generate electricity, while electricity could also be generated directly from photovoltaics (PV). To assess the benefits from solar energy from such systems, energy/exergy, environmental, or economic criteria has been used. For example, solar parabolic trough collectors (PTCs) were used to preheat compressed air and to decrease the natural gas consumption in a tri-generation system (Wang, Lu, Li, Lior, & Li, 2019), leading to energy efficiencies of 83.6% and 66.0% in two working conditions. In another study, coupling to the organic Rankine cycle, a solar-assisted system dropped the fossil fuel use by 12.4% (Wu et al., 2019). System performance analyses have been extended with life-cycle assessment (LCA) methods (Sajid & Bicer, 2021) and also adding an ecological view to the analysis (Egilmez, Kucukvar, & Park, 2016).

LCA methods estimate the energy consumption and pollutant emissions from the cradle to grave considering all intermediate process steps such as material acquisition, system operation, and recycling (J. Ren, 2018). LCA has been applied in energy systems to evaluate energy (Hasanzadeh, Chitsaz, Mojaver, & Ghasemi, 2021) and emergy (Babaelahi, Rafat, & Mofidipour, 2019) performance. Compared to conventional separate and tri-generation systems (Luo et al., 2020), the life-cycle energy consumption of renewable energy driven system could be decreased by nearly 10%, and 15%, and the carbon emissions by 80% and 20%, while the total cost increased. LCA will also be helpful as part of the optimization process when searching for ideal system configurations. To minimize the pollutant emissions of a PV assisted tri-generation system (Wang, Yang, Mao, Sui, & Jin, 2015) used the total environmental impact as objective function in their optimization showing that the emissions from operating the system, material acquisitions, and the system construction constituted the largest part of the pollutants. The optimization process can also include several criteria simultaneously, e.g. combining environmental aspects and techno-economic methods (Wang et al., 2021) e.g. to evaluate the life-cycle exergo-economic performance (Mehrabadi & Boyaghchi, 2021). For example, (Chen, Xu, Wang, Lund, Han, et al., 2022) optimized a solar-assisted tri-generation system with such approach yielding 50.1% energy cost savings, 43.5% exergo-environmental savings and 99.8% matching performance. However, these studies are often related to the specific investment cost of the devices, which may vary in different regions. By calculating the cumulative exergy consumption of specific processes to evaluate the ecological performance one could eliminated the investment costs in the analysis. This approach will also be employed here.

The cumulative exergy assessment has been used to compare the sustainability of energy products (Szargut, 1987). As a further improvement, the specific thermo-ecological cost (Stanek & Czarnowska, 2018) was defined and was used to analyse renewable power plants (Stanek, Czarnowska, Gazda, & Simla, 2018; Stanek, Mendecka, Lombardi, & Simla, 2018), renewable power driven heat pumps (Stanek, Simla, & Gazda, 2019), hydrogen production (Erzen, Ünal, Açıkkalp, & Hepbasli, 2021), absorption heat pumps (Ahmadi, Ahmadi, Mehrpooya, & Sameti, 2015), and especially co-generation and poly-generation systems (Gładysz, Saari, & Czarnowska, 2020). Integrating the thermo-ecological concept into a techno-economic method, the specific thermo-ecological cost (STEC) was illustrated by (Chen, Hua, Wang, & Lund, 2021). Chen et al. (2019) optimized (Chen, Wang, Ma, & Gao, 2019) a photovoltaic/solar thermal coupled trigeneration system resulting with this method obtaining as 2.36 J/J minimum cost. STECs of multiple energy products from the solar-assisted tri-generation system are optimized simultaneously in the present study.

Optimization of the thermo-ecological cost of multiple products for a solar thermal and PV assisted energy system considering the energy level from an ecological view is the novelty of the study. The main contributions here contain the following: (1) A solar thermal and PV integrated energy system (STP-IES) is defined to meet multiple types of energy demand by employing a water-cooled chiller with a high energy performance; (2) Equivalent emissions are used to calculate the exergy consumption of harmful pollutants; (3) The system performance with and without the energy level is compared; (4) The specific thermo-ecological costs of the energy are analyzed against key parameters.

2 Solar thermal and photovoltaic integrated energy system

In this section, the energy flowcharts (Sec. 2.1), thermal models and operating modes of the devices (Sec. 2.2) are described.

2.1 Energy flowcharts

The energy flowcharts of the system is illustrated in Fig. 1. In addition to the conventional combined cooling, heating, and power system containing a gas turbine (GT) (Ebrahimi-Moghadam et al., 2021), an AHP cycle is used in the integrated energy system concept to meet the continuous energy demand of the building. The AHP is cascaded with utilization of natural gas (state 2), electricity (state 5), and exhaust gas from the GT (state 3). The detailed flows of the GT and AHP are ignored such as the compressor and expander.

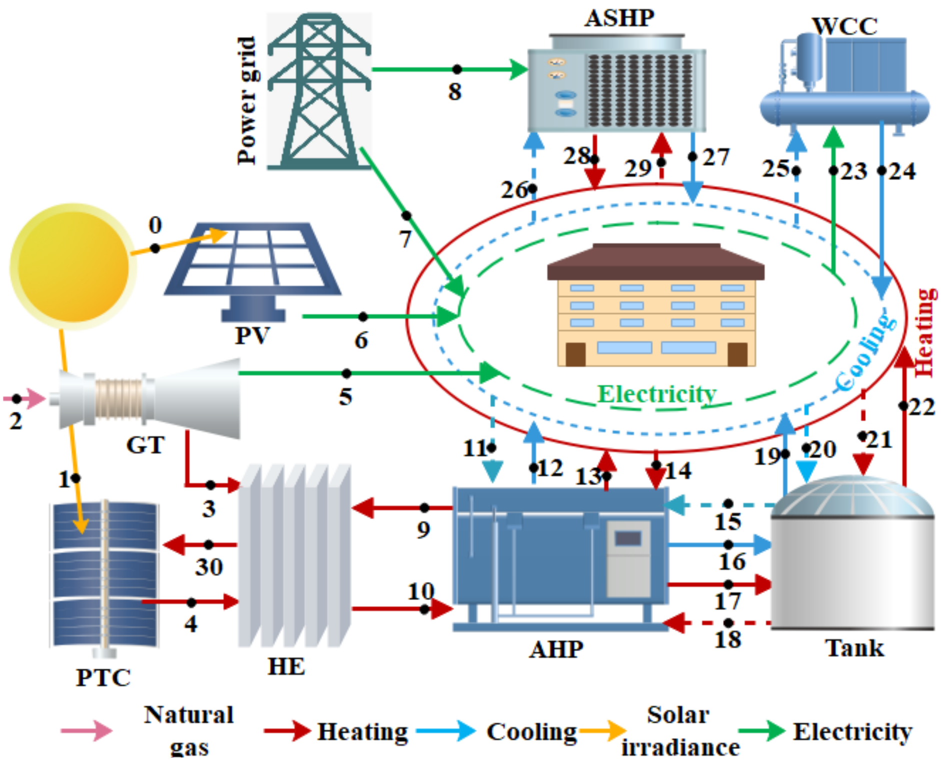

Fig. 1. Energy flowcharts of the solar thermal and photovoltaic integrated energy system: GT = Gas turbine,

PV = Photovoltaic, PTC = Parabolic trough collector, HE = Heat exchanger, AHP = Absorption heat pump, ASHP = Air-source heat pump, WCC = Water-cooled chiller.

Other energy subsystems include the solar PTC and PV to convert solar irradiance (states 0 and 1) into thermal energy (state 4) and electricity (state 6). The heat exchanger (HE) is employed here to produce steam and drive the double-effect AHP to produce chilled and heating water, and the WCC meets the remaining demand of chilled water. The system outputs and the building demands vary due to the environmental parameters and operating schedules, for which reason a and water tank is use to balance the demand and supply. The power grid will supply the electric deficit during high electricity demand conditions. The ASHP is used to supply both heat and chilled water employing grid electricity. The overall electricity demand is satisfied by the GT, PV, and power grid; the heating/cooling demand is met by the AHP, tank, and ASHP, while the WCC will produce chilled water only. The solar electricity output may occasionally exceed the electricity demand that could lead to some curtailment of PV output. The system is well suited for high cooling and low heating conditions due to the high performance of the cooling devices.

To analyze the exergy performance in Section 3, the basic temperatures of states in Fig. 1 need to be defined. In the present study, the outlet temperature of the exhaust gas from the GT is set at 470°C (Chen, Wang, & Lund, 2020b). To match the operating temperature of the AHP and reach a higher energy efficiency of the PTC, the temperature difference of solar steam and stem to the AHP are set to 20°C and 15°C (Chen, Xu, Zhao, Wang, & Lund, 2021). The temperature difference of chilled and heating water are 5°C and 10°C , respectively (Chen, Xu, Zhao, et al., 2021). The temperatures are listed in Table 1.

Table 1. Basic temperatures of states in Figure 1.

Items	State in Fig. 1	Temperature, °C
Exhaust gas	3	470
Steam from PTC	4	170
Steam to PTC	30	150
Steam to AHP	10	150
Steam from AHP	9	135
Heating water	13, 17, 22, 29	50
	14, 18, 21, 28	40
Chilled water	12, 16, 19, 24, 26	7
	11, 15, 20, 25, 27	12

2.2 Operating modes of devices

The thermal principles of the devices are summarized in Table A1 in Appendix. In the simulation, steady state is assumed to simplify the calculation process. The models are validated by comparing the simulated results to other studies: For PTC (Xu, Chen, Wang, Lund, & Wang, 2022) for GT cycle; for PV (Chen, Hu, et al., 2022), (Chen, Xu, Zhao, et al., 2021);for AHP cycle , WCC and ASHP, (Jiang, 2019); the HE and the tank are handled as black boxes using constant charging and discharging efficiencies.

The hybrid system consists of multiple devices, for which reason it is essential also to describe the operating modes to meet the energy demands. Moreover, to yield a higher overall performance in tri-generation system, the electricity demand is first satisfied by the PV, followed by the GT, and last by the power grid in the (Xu et al., 2022). The operating modes are shown in Table 2.

Table 2. On and off conditions of the units in meeting the electricity demand.

Units	$E_t^j < E_{PV}^j$	$E_{PV}^j + E_{GT}^{min} > E_t^j > E_{PV}^j$	$E_{PV}^j + E_{GT}^{max} > E_t^j > E_{PV}^j + E_{GT}^{min}$	$E_t^j > E_{PV}^j + E_{GT}^{max}$
PV	On	On	On	On
GT	Off	Off	On	On
Power grid	On	On	Off	On

where E_t^j, E_{PV}^j are the total electricity demand and solar electricity in j^{th} hour. E_{GT}^{max}, E_{GT}^{min} represent the hourly maximum and minimum electric output of GT, respectively.

The operating schedules for the cooling and heating demand is displayed in Fig. 2. The water-cooled unit is prioritized for chilled water due to the higher COP. The deficit is supplied by the AHP, tank, and ASHP. Except for the WCC for cooling, the system has a similar operating schedule for heating water production: AHP, tank, and ASHP.

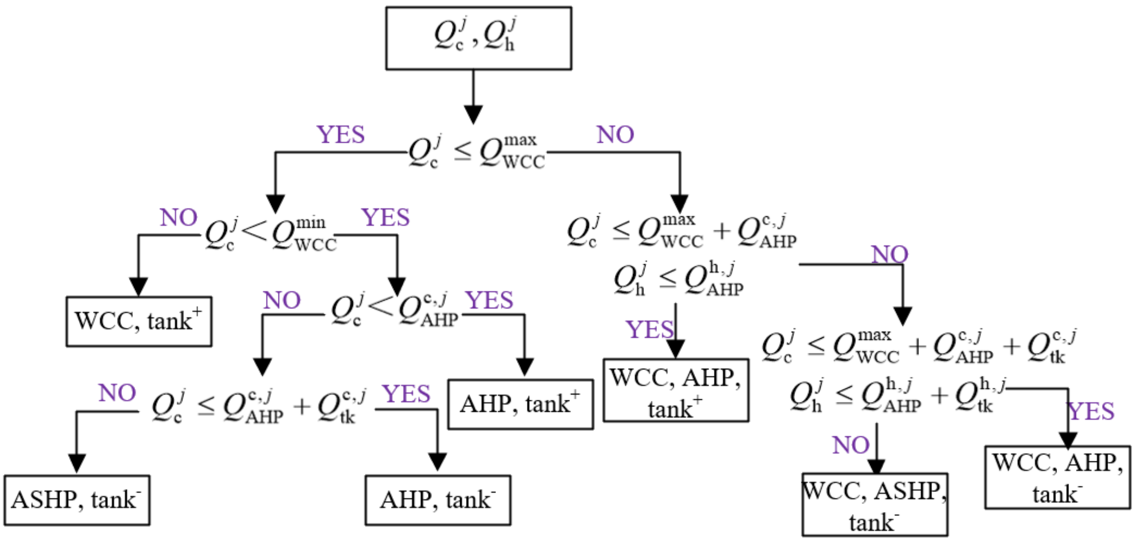

Fig. 2. Operating conditions of devices to meet the cooling and heating demands ('+' means charge and '-' discharge of the tank).

3. Thermo-ecological cost optimization method

In Section. 3.1, the thermo-ecological cost method is described considering the energy level of the products from an ecological point of view. Section 3.2. describes the optimization approach used to explore optimal configurations of the STP-IES.

3.1 Thermo-ecological cost assessment

In the thermo-ecological cost method, the cumulative exergy consumption for specific products are analyzed, which are related to the direct non-renewable exergy consumption, raw materials, byproducts, harmful pollutants, etc. Some assumptions are made here: (1) The import of materials is ignored; (2) No semi-finished and by-products are present in the system studies; (3) The main harmful pollutants are carbon dioxide, sulfides, and dust (Chen, Hua, et al., 2021). Then, the cumulative exergy consumption of the i^{th} process (CExE_i) can be written as follows (Stanek, Simla, Rutczyk, et al., 2019):

$$\mathrm{CExE}_i = \mathrm{CExE}_h + \mathrm{CExE}_{\mathrm{NE}} + \mathrm{CExE}_{\mathrm{p}} \tag{1}$$

where CExE_h, $\mathrm{CExE}_{\mathrm{NE}}$, and $\mathrm{CExE}_{\mathrm{p}}$ are the cumulative exergy consumption of h^{th} process, the non-renewable energy, and cumulative compensating exergy consumption caused by harmful pollutants, respectively.

The utilized energy in this study is natural gas, grid electricity, and solar irradiance, for which the cumulative exergy consumption is 1.04 J, 3.60 J, and 0.02 J per Joule exergy (Stanek & Czarnowska, 2018). Additionally, the compensated exergy consumption of pollutant emissions is summarized in Table 3.

Table 3. Compensated exergy consumption of pollutant emissions (Stanek & Czarnowska, 2018).

Pollutants	Compensate cost, MJ/kg
Carbon dioxide	97.82
Sulfur dioxide	71.88
Dust	53.42

The equivalent carbon, sulfur, and dust emissions over the life-cycle are estimated considering the emissions from an ecological point of view (Chen, Hua, et al., 2022):

$$\mathrm{CExE}_{\mathrm{p}} = \mathrm{CEC}_{\mathrm{CO_2}} \cdot m_{\mathrm{eqv.CO_2}} + \mathrm{CEC}_{\mathrm{SO_2}} \cdot m_{\mathrm{eqv.SO_2}} + \mathrm{CEC}_{\mathrm{dust}} \cdot m_{\mathrm{eqv.dust}} \tag{2}$$

Where CEC is the compensated exergy consumption and m isthe mass of harmful pollutants, respectively. The details of equivalent emissions are summarized in Tables A2 -A4 in the Appendix.

The cumulative exergy consumption of the equivalent emissions of the different devices is divided into two parts based on the share of cooling and heating conditions enabling to explore the thermo-ecological performance of chilled water and heating water. The heating ratio (γ) is defined as the operating time of the heating mode to 8760 hours over the whole year. The cumulative compensated exergy consumption for the heating and cooling modes are the following:

$$\mathrm{CExE_p^h}=\mathrm{CExE_p}\cdot\gamma \tag{3}$$

$$\mathrm{CExE_p^c}=\mathrm{CExE_p}-\mathrm{CExE_p^h} \tag{4}$$

Then, the cumulative exergy balances of the devices considering the energy level are summarized in Table 4.

Table 4. Cumulative exergy balance and auxiliary equations.

Device	Cumulative exergy balance equations	Auxiliary equation
PV	$\mathrm{CExE_0^{c/h}}+\mathrm{CExE_{PV,p}^{c/h}}=\mathrm{CExE_6^{c/h}}$	
PTC	$\mathrm{CExE_1^{c/h}}+\mathrm{CExE_{PTC,p}^{c/h}}=\mathrm{CExE_{4-30}^{c/h}}$	
GT	$\mathrm{CExE_2^{c/h}}+\mathrm{CExE_{GT,p}^{c/h}}=\mathrm{CExE_5^{c/h}}+\mathrm{CExE_3^{c/h}}$	$\dfrac{\mathrm{CExE_5^{c/h}}\cdot\mathrm{ExE_3^{c/h}}}{\mathrm{CExE_3^{c/h}}\cdot\mathrm{ExE_5^{c/h}}}=\dfrac{\mathrm{EL_5}}{\mathrm{EL_3}}$
WCC	$\mathrm{CExE_{23}^{c}}+\mathrm{CExE_{WCC,p}^{c/h}}=\mathrm{CExE_{24-25}^{c}}$	
AHP	$\mathrm{CExE_{9-10}^{c}}+\mathrm{CExE_{AHP,p}^{c}}=\mathrm{CExE_{11-12}^{c}}+\mathrm{CExE_{15-16}^{c}}$ (Cooling mode)	
	$\mathrm{CExE_{9-10}^{h}}+\mathrm{CExE_{AHP,p}^{h}}=\mathrm{CExE_{13-14}^{h}}+\mathrm{CExE_{17-18}^{h}}$ (Heating mode)	
Tank	$\mathrm{CExE_{15-16}^{c}}+\mathrm{CExE_{tk,p}^{c}}=\mathrm{CExE_{19-20}^{c}}$ (Cooling mode)	
	$\mathrm{CExE_{17-18}^{h}}+\mathrm{CExE_{tk,p}^{h}}=\mathrm{CExE_{21-22}^{h}}$ (Heating mode)	
ASHP	$\mathrm{CExE_{8}^{c}}+\mathrm{CExE_{ASHP,p}^{c}}=\mathrm{CExE_{26-27}^{c}}$ (Cooling mode)	
	$\mathrm{CExE_{8}^{h}}+\mathrm{CExE_{ASHP,p}^{h}}=\mathrm{CExE_{28-29}^{h}}$ (Heating mode)	
HX	$\mathrm{CExE_3^{c/h}}+\mathrm{CExE_{4-30}^{c/h}}+\mathrm{CExE_{HE,p}^{c/h}}=\mathrm{CExE_{9-10}^{c/h}}$	

The subscripts refer to the states in Fig. 1. EL means energy level.

Similar to the specific exergy-economic cost of the products(Babaelahi et al., 2019), the specific thermo-ecological cost (STEC) of the product is related to the cumulative exergy consumption and exergy as follows:

$$\mathrm{STEC}_h=\frac{\mathrm{CExE}_h}{\mathrm{ExE}_h} \tag{5}$$

Based on the temperatures in Table 1, the exergy of each state can be calculated as follows:

$$\mathrm{ExE}_Q = Q\cdot(1-\frac{T_{\mathrm{std}}}{\overline{T}}) \tag{6}$$

where Q, and $\overline{T}$ are the mean thermal energy and average temperature.

Finally, the specific thermo-ecological cost of cooling, heating, and electricity over the year are calculated as follows:

$$\mathrm{STEC_c} = \frac{\mathrm{STEC_{11-12}\cdot ExE_{11-12} + STEC_{19-20}\cdot ExE_{19-20} + STEC_{24-25}\cdot ExE_{24-25} + STEC_{26-27}\cdot ExE_{26-27}}}{\mathrm{(ExE_{11-12} + ExE_{19-20} + ExE_{24-25} + ExE_{26-27})}} \tag{7}$$

$$\mathrm{STEC_h} = \frac{\mathrm{STEC_{13-14}\cdot ExE_{13-14} + STEC_{21-22}\cdot ExE_{21-22} + STEC_{28-29}\cdot ExE_{28-29}}}{\mathrm{(ExE_{13-14} + ExE_{21-22} + ExE_{28-29})}} \tag{8}$$

$$\mathrm{STEC_E} = \frac{\mathrm{STEC_6\cdot ExE_6 + STEC_5\cdot ExE_5 + STEC_7\cdot ExE_7}}{\mathrm{(ExE_6 + ExE_5 + ExE_7)}} \tag{9}$$

The specific cost of the hybrid is given by:

$$\mathrm{STEC_{IES}} = \frac{\mathrm{STEC_E\cdot ExE_E + STEC_c\cdot ExE_c + STEC_h\cdot ExE_h}}{\mathrm{(ExE_E + ExE_c + ExE_h)}} \tag{10}$$

where $\mathrm{STEC_c}$, $\mathrm{STEC_h}$, $\mathrm{STEC_E}$, and $\mathrm{STEC_{IES}}$ represent the specific thermo-ecological cost of cooling, heating, electricity, and the hybrid system.

3.2 Optimization method

The minimum specific thermo-ecological cost of the products in the STP-IES is searched with a multi-objective optimization process in which the specific costs of cooling, heating, and electricity are set as the objectives of the optmization:

$$\begin{cases} \mathrm{Min\ STEC_c} \\ \mathrm{Min\ STEC_h} \\ \mathrm{Min\ STEC_E} \end{cases} \tag{11}$$

The outputs from the PTC and PV are easily affected by the installed collector areas affecting the performance of the hybrid system. To ensure the continuous operation of the system, the GT can produce electricity and exhaust gas to drive the AHP, but its capacity would also influence the thermo-ecological cost of the products. Then, the capacity of WCC influences the operating modes for the chilled water and a higher capacity of the water tank would enlarge the matching performance of the system consuming more compensated cumulative exergy. The decision variables in this study are set as follows:

$$[C_{GT}, C_{WCC}, C_{tk}, A_{PTC}, A_{PV}] \tag{12}$$

where C, and A are the capacity and the area of the devices, respectively. The ranges of the variables are given in Section 4 based on a sample case.

The genetic algorithm (NAGA-II) validated in (Chen, Li, Hua, Lund, & Wang, 2022) is employed here to explore the configurations of hybrid system. The validation was done by comparing the results with values optimized by the particle swarm algorithm (Yuan, Liu, & Bucknall, 2021). The parameters values used here are summarized in Table A5 in the Appendix. Moreover, the inequal and equal constraints of the algorithm are limited by the parameters in Fig. 1, and the technical parameters in Table A1 (Xu et al., 2022).

With the NAGA-II, a set of Pareto frontiers are obtained. To select the ideal configuration of the system, the maximum sustainable index (SI) is searched based on the following processes: (1) Standardization of values (Chen, Wang, & Lund, 2020a); (2) Weights acquisition using coefficient variable method (Chengjiang, Mingguang, Yinting, & Rui, 2014):

(1) Standardization of values:

$$\overline{x_k} = \frac{X_{min}}{X_k} \tag{13}$$

(2) Weights of index:

$$\omega_k = \frac{V_k}{\sum V_k} \tag{14}$$

(3) Sustainable index (SI):

$$SI = \sum X_k \cdot \omega_k \tag{15}$$

where $\overline{x_k}$, X_k, V_k and ω_k are the mean normalized value, value, variable coefficient, and weight of the k^{th} index.

4. Results and discussion based on a sample case

To explore the thermo-ecological cost performance using the method in Section 3, a sample case with low heating and high cooling demand is selected. The energy demand constitutes of market, residential, and market buildings. The chilled and heating water demands in the cooling and heating season (Chen, Xu, Wang, Lund, & Wang, 2022) were simulated in the DesT software (Delač, Pavković, & Lenić, 2018) by our group (Chen, Li, et al., 2022) using structural parameters and electrical schedules of equipment given in (Xu et al., 2022). The monthly electricity, chilled, and heating water demands are shown in Fig. 3.

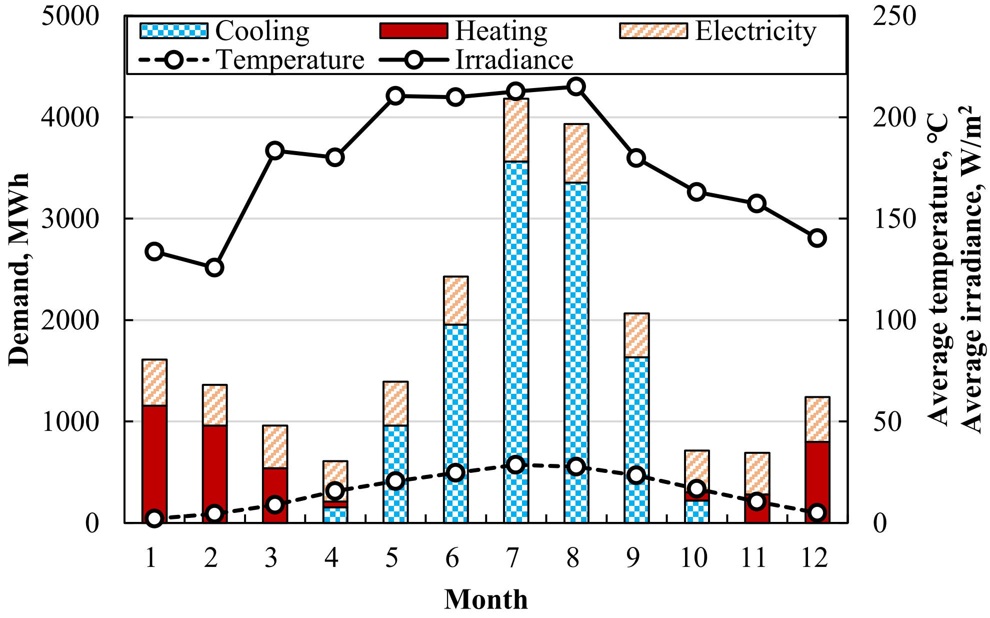

Fig. 3. Energy demand and environmental parameters of the case (Chen, Li, et al., 2022).

Based on the demands in Fig. 3, the ranges for the decision variables are listed in Table 5.

Table 5. Ranges of decision variables.

Capacity/Area	Lower range	Upper range
GT, kW	0	2000
PV, m^2	0	5000
PTC, m^2	0	5000
Tank, kWh	0	6000
WCC, kW	0	9000

To compare the optimization results with other studies, two methods are considered:

- Modified method: The energy levels of the products in Table 4 are considered;
- Conventional method: The energy levels of the products is ignored (Chen, Zhao, Xu, Wang, & Lund, 2021).

4.1 Optimization results

Figure 4 shows the optimized values of the decision variables, and Figs. 4(a) and 4(b) explicate the populations of the modified method. The optimized variables with the conventional method are shown Figs. 4(c) and 4(d). In Fig. 4(a), the optimized capacities of the GT are almost 1000 kW, and most of the capacities of the tank are > 5000 kWh, while half of all WCC are < 2000 kW. Contrary to the higher capacity in Fig.

4(a), some of the capacities of GT with the conventional method in Fig. 4(c) are less than 500 kW, and the tank size is mainly concentrated between 4000 kWh and 6000 kWh. However, most of the optimized capacity values of WCC in Fig. 4(c) have a higher range (from 0 to 8000 kW) than that of the modified method.

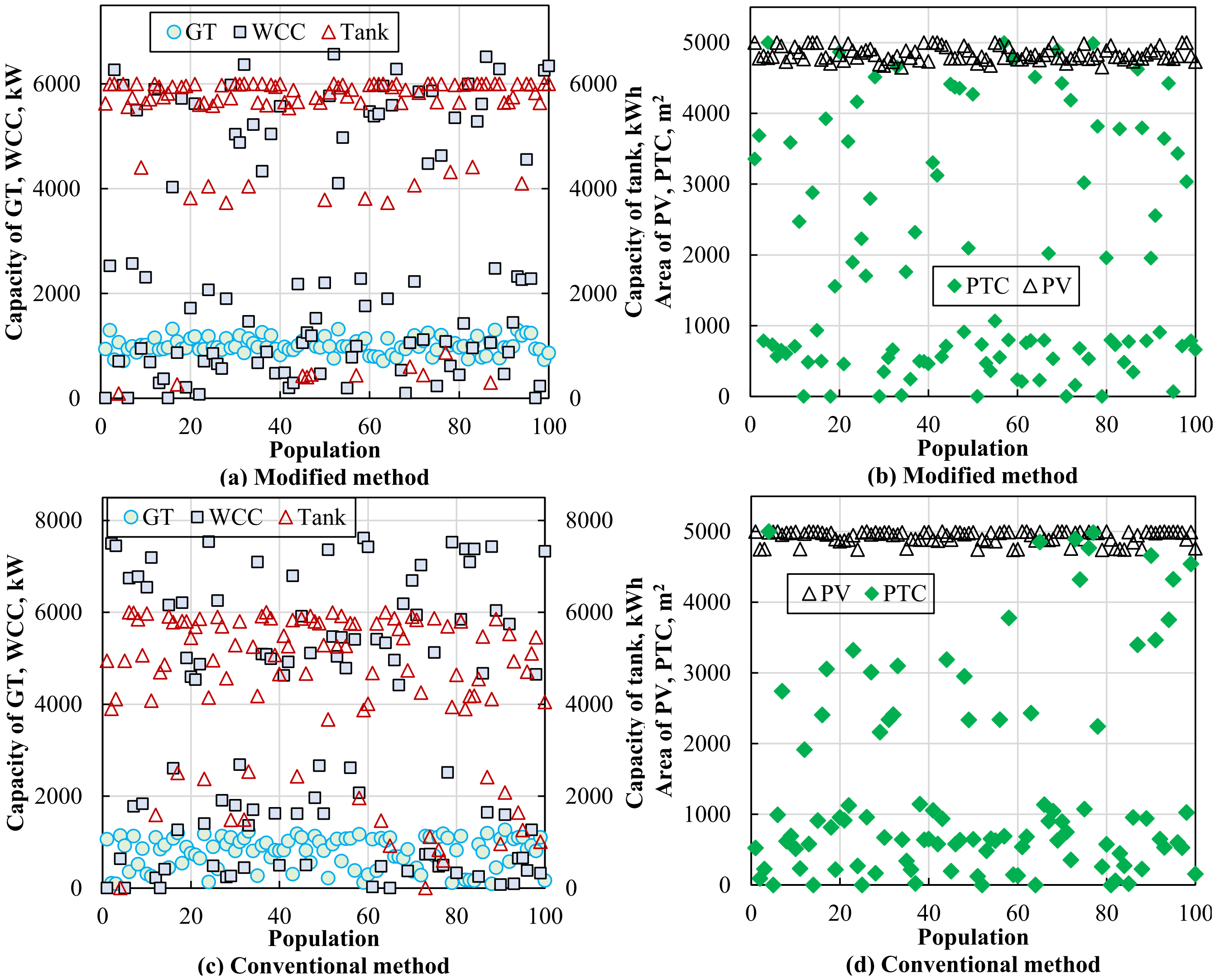

Fig. 4. Optimized populations of the decision variables.

In Figs. 4(b) and 4(d), the optimized areas of the PV installations with both methods are above 4500 m^2, while half of the installed areas of the PTC are less than 1000 m^2, especially when using the conventional method.

The maximum, minimum, and average capacities of the optimized variables are given in Table 6. The average capacity of the GT with modified method is 68 kW lower than with the conventional method, although the maximum and minimum capacities are 57 and 619 kW higher. The conventional method yields a higher maximum and average capacity of the WCC although the minimum values are 0 with both methods. The maximum size of the tank, PV, and PTC with both methods is equal to the upper capacity value given in Table 5, or 6000 kWh, and 5000 m^2, respectively. The optimized areas of PV range from 4650 m^2 to 5000 m^2 with the modified method, while the spread of the PTC area is much larger from 0 to 5000 m^2 lower. This indicates the more important role of PV than PTC for the integrated system.

Table 6. Maximum, minimum, and average values of optimized variables with the two methods.

		GT, kW	WCC, kW	Tank, kWh	PV, m^2	PTC, m^2
Modified method	Maximum value	1325	6569	6000	5000	5000
	Minimum value	712	0	90	4650	0
	Average value	1006	2757	5097	4835	1896
Conventional method	Maximum value	1268	7621	6000	5000	5000
	Minimum value	93	0	0	4743	0
	Average value	780	3573	4422	4929	1367

Using Eqs. (7)-(9), the optimized objective functions are illustrated in Fig. 5, both with the modified and conventional method. Increasing the specific cost of electricity for the first one third of the population, the specific thermo-ecological cost for heating and chilled water decreases. The main reason for this is the increasing capacity of the water-cooled chiller. When the capacity of the WCC is 0, the chilled water is met by the AHP, tank, and ASHP using grid electricity with a higher STEC of 3.6. The share of the WCC increases with a higher COP, and the grid electricity consumption reduces, but may also lead to a lower capacity of ASHP, which results in a lower compensate exergy consumption in both the cooling and heating mode, and consequently the specific heating cost is also decreased. Then, the specific thermo-ecological cost for the water product including heating and chilled water is higher than the cost of electricity, due to the complex energy flows for heating/cooling production in Fig. 1, especially for chilled water.

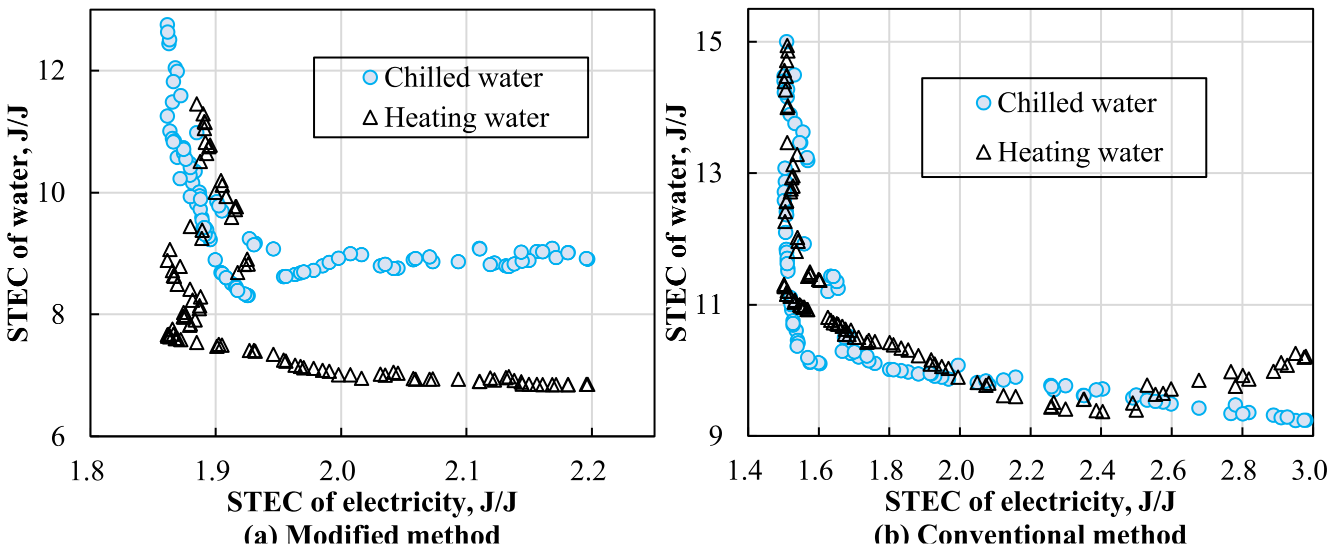

Fig. 5. Pareto solutions of the objectives.

Compared to modified method, the conventional method gives a wider range for the electricity cost from 1.50 to 2.98 (Table 7), while the thermo-ecological cost of electricity considering the energy level ranges from 1.96 to 2.2. However, considering the energy level between the electricity and exhaust gas from GT, more cumulative exergy consumption is allocated to electricity, resulting in an average specific cost of 0.36 J/J higher than the cost in the conventional method. On the other hand, the thermo-ecological price of chilled and heating water have a narrower range when using the modified method (from 8.31 J/J to 12.75 J/J for chilled water, and 6.85 J/J to 11.45 J/J for heating water), due to the lower cumulative exergy consumption of exhaust gas, which is used to drive the AHP to produce a part of the water products The average price of cooling/heating using conventional method is 1.43 J/J and 2.39 J/J lower, respectively, than with the modified method.

Table 7. Maximum, minimum, and average values of STEC with the two methods.

	Item, J/J	Modified method	Conventional method
Electricity	Maximum value	2.20	2.98
	Minimum value	1.86	1.50
	Average value	1.96	1.89
Heating water	Maximum value	11.45	14.84
	Minimum value	6.85	9.37
	Average value	8.13	11.06
Chilled water	Maximum value	12.75	15.00
	Minimum value	8.31	9.24
	Average value	9.57	10.91

Using the variable coefficient method, the weights of cooling, heating, and electricity cost are 0.34, 0.49, and 0.17 with the modified method, and the corresponding values are 0.28, 0.27, and 0.45 for the conventional method. The ideal configurations of the STP-IES are then determined using these values and are listed in Table 8. Except for the solar installation areas, especially the solar thermal PTC, the configured capacities with the modified method are larger than the capacities with the conventional method. The differences in the capacities of ASHP, HE, and AHP are the largest, or > 1300 kW, while the difference of the GT is the lowest, or < 200 kW. Due to the higher capacity of theWCC and GT, the corresponding areas of the PV and PTC with the modified method are 211 m^2 and 2178 m^2 lower.

Table 8. Ideal configurations with the modified and conventional method.

Capacity/Area	Modified method	Conventional method
GT, kW	1253	1093

PV, m^2	4771	4982
PTC, m^2	68	2246
Tank, kWh	6000	5695
WCC, kW	4560	2517
ASHP, kW	2629	1351
HE, kW	3023	1742
AHP, kW	5224	3010

With the ideal capacities in Table 8, the specific thermo-ecological costs of the products are summarized in Table 9. Concerning the cost of solar electricity, its cost in the heating mode, 0.865 J/J, is lower than the cost in the cooling mode, 1.057 J/J, which is due to the from the higher electrical efficiency due to lower ambient temperature, while the thermal efficiency of PTC in the heating mode is lower than the efficiency during cooling, leading to a high specific cost of solar steam, 0.723 J/J. For the products from the GT, the STEC of electricity in the heating and cooling conditions is 1.256 J/J and 0.96 J/J higher than the STEC of the solar electricity with the modified method, and 0.736 J/J, and 0.516 J/J higher with the conventional method, respectively. Additionally, the STEC of the exhaust gas considering the energy level is 0.661 J/J cheaper than the cost with the conventional method in the heating mode, and 0.680 J/J lower in the cooling conditions.

Table 9. Specific thermo-ecological costs of the products with the modified and conventional method.

	Item	Modified method, J/J	Conventional method, J/J
Heating condition	Electricity from PV	0.865	0.865
	Heating from PTC	0.723	0.723
	Electricity from GT	2.121	1.601
	Exhaust gas from GT	0.940	1.601
	Total electricity	1.859	1.459
	Heating from AHP	3.995	5.798
	Heating from Tank	23.099	43.554
	Heating from ASHP	33.482	41.282
	Total heating	7.129	11.427
Cooling condition	Electricity from PV	1.057	1.057
	Heating from PTC	0.541	0.547
	Electricity from GT	2.017	1.573
	Exhaust gas from GT	0.893	1.573
	Total electricity	2.030	1.633
	Cooling from AHP	6.320	8.980
	Cooling from Tank	132.850	113.390
	Cooling from ASHP	44.326	30.433
	Cooling from WCC	5.967	4.907
	Total cooling	8.699	10.193
Whole year	Electricity	1.970	1.569
	Hybrid system	2.691	2.644

In the heating mode, the STEC of electricity is 0.4 J/J higher when using the modified method, but the cost of heating water is cheaper both for the AHP, tank, and ASHP. The heating water from the AHP and tank is generated by the exhaust gas or solar thermal heat, but the specific cost of water from the tank is almost 6-times higher than the cost from the AHP with the modified method and 8-times higher with the conventional method, because of the higher capacities of the tank and most of the charged heating water being wasted to the environment resulting from the lower heating demand. Considering the energy level, the heating water from the ASHP is the most expensive: it is 30 J/J and 10 J/J higher than the cost from the AHP and tank (modified method), while the cost from tank accounts for the largest, 43.554, J/J with conventional method, due to the higher cost of exhaust gas. In total, the thermo-ecological cost of the heating water is 7.129 J/J with the modified method, which is 4.298 J/J lower than with the conventional method.

As Fig. 2 shows, the cooling demand is firstly satisfied by the WCC using electricity from the GT and PV, and it yields the cheapest chilled water, or 5.967 J/J and 4.907 J/J with the modified and conventional method. The cost ranking of the STEC of the chilled water from the other devices is similar to the heating mode with the conventional method: The AHP generates the cheapest product followed by the ASHP, while the cost of the chilled water from the tank is very high, or 132.850 and 113.390 J/J for the two methods. This is caused by the operating schedules in cooling conditions and because most of the chilled water is supplied by the WCC and AHP, while the tank wastes a larger part of the product. In total, the STEC of the chilled water is 1.57 J/J higher than the cost of the heating water with the modified method, but the specific cost is 1.234 J/J cheaper in the conventional method, due to the cheaper product from the WCC and the ASHP. The STEC of electricity over the whole year is 1.970 and 1.569 J/J for the two methods. Using Eq. (10), the STEC of the proposed system with the modified method is 0.047 J/J higher than the cost in the conventional method, resulting from the higher electricity and lower cooling/heating exergy of the products, although the water demand is higher (Fig. 3).

4.2 Performance in heating and cooling modes

In the next, the performance in the cooling/heating modes (Sec. 4.2), and annual performance of the devices (Sec. 4.3) are described followed by a discussion (Sec. 4.4).

4.2.1 Heating mode

Based on the configurations in Table 8, the shares of the devices for heating water and electricity production in the heating mode are shown in Fig. 6: Figs. 6(a) and 6(b) for the modified method, and Figs.

6(c) and 6(d) for the conventional method.

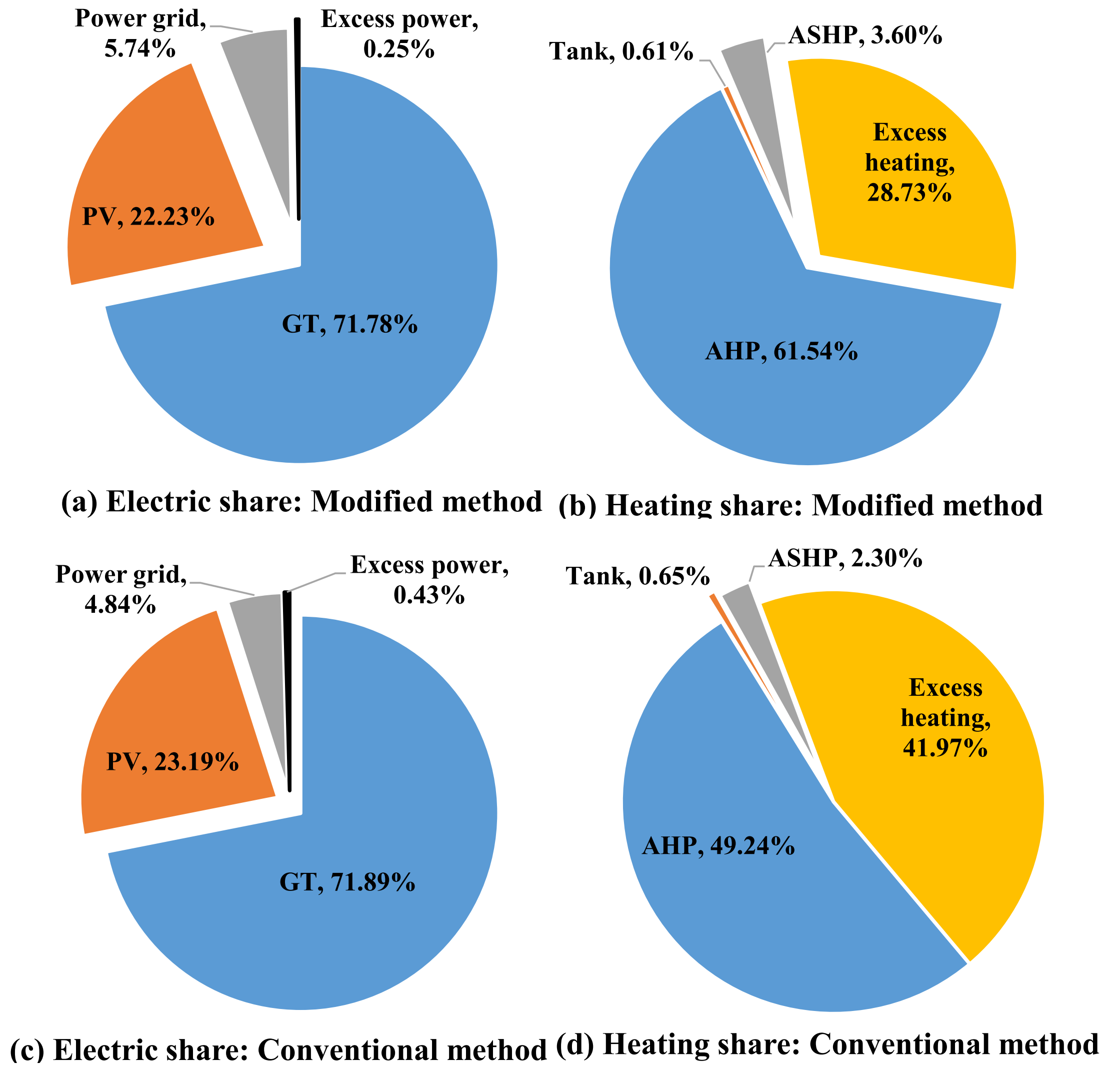

Fig. 6. Share of electricity and heat in heating conditions.

With 4771 m^2 PV panels, 569.3 MWh solar electricity is generated in the heating mode and 98.8% of that is used to meet the electricity demand, while 0.25% in Fig. 6(a) is wasted due to the supply and demand mismatch. The GT share of total production is 71.78% can meet most of the demand. The power grid can supply the deficit or 5.74% of the total electricity outputs. Only 33% of the grid electricity go for meeting the electricity demand, while a larger part goes to the ASHP to produce heating water. The descending order of the devices for electric production are the GT, PV, and power grid.

For heating production with conventional method in Fig. 6(b), the AHP unit is responsible for 61.54% of the total heating production could afford 93.6% of total heating demand, and followed by the ASHP with 5.5% share, while 0.9% comes from the water tank. 28.7% of the heating water is wasted in the tank due to the lower heating demand and limited capacity of the tank, which causes a higher STEC for the heating water, or

23.099 J/J in Table 9.

Compared to Fig. 6(a), the system with the conventional method in Fig. 6(c) generates 15.5 MWh less electricity. With nearly 200 m^2 more of PV panels, the system has a higher solar electricity output, or 25.2 MWh in the heating mode, while the output of the GT is 8.2 MWh lower, although the share is 0.11% higher in Fig. 6(c). Moreover, the share of the power grid is 0.9% lower than in Fig. 6(a), and 68.6% of that is used in the ASHP.

Owing to the higher area of PTC, 2246 m^2, 41.97% of the total heating is lost in the tank, which results in the highest STEC of heating water of all devices, or 43.554 J/J. As a result, the contribution of the ASHP is 42.4 MWh lower than in Fig. 6(b), which accounts for 2.30% of the total heating production. Moreover, heating water provided by theAHP in this condition is 57.8 MWh lower than in Fig. 6(b), although the solar thermal output is higher. Solar thermal is easily affected by weather parameters, while the heating demand is often needed at night, which is directly influenced by the capacity of the GT. It could be concluded that the PTC has a lower contribution in the heating mode due to the intermittency of solar irradiance and operating schedules of heating water.

4.2.2 Cooling mode

In the cooling mode, the electricity demand is satisfied by the GT, PV, and grid, while the cooling demand is met by theWCC, tank, AHP, and ASHP. The corresponding shares of the devices are shown in Fig. 7.

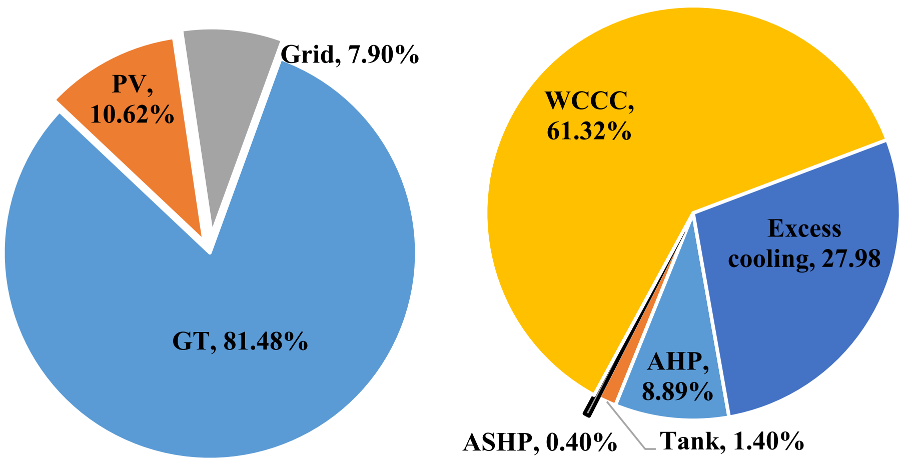

(a) Electric share: Modified method (b) Cooling share: Modified method

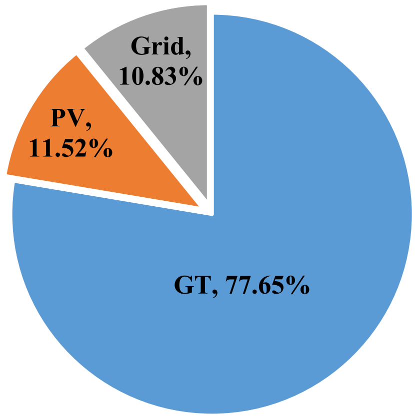

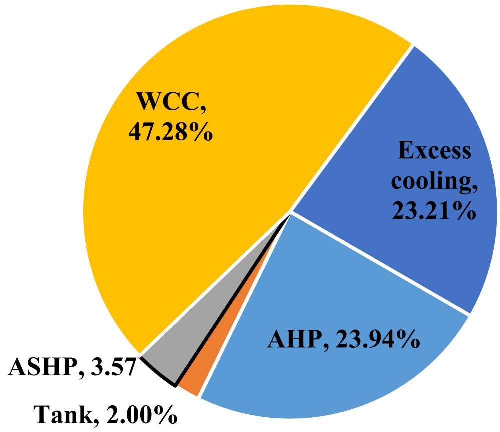

(c) Electric share: Conventional method (d) Cooling share: conventional method

Fig. 7. Electric and cooling share in cooling condition.

Contrary to the electricity share in theheating mode, the wasted solar electricity in the cooling condition is 0, due to the higher electricity demand caused by the building and the WCC. With the modified method shown in Fig. 7(a), the total electricity demand is 172.6 MWh higher than the demand with the conventional method. 81.48% is supplied by GT and 10% by the PV. The share of the grid electricity consumption is 7.9% of the total demand, but only 7.7% of it is used to drive the ASHP to generate the last part of the chilled water. The share of the GT in Fig. 7(c) decreased by 3.83% due to lower capacity, while the share of PV is increased to 11.5%. 10.8% of the demand comes from the power grid, and 47.1% of the electricity flows to the ASHP to supply the deficit of cooling due to the lower WCC capacity.

For chilled water production in Figs. 7(b) and 7(d), the WCC shares is 61.3% and 47.3% of the total cooling output could meet at least 85% and 61% of the total cooling demand. Then, 1462 MWh, and 3692 MWh cooling demand is fulfilled by the AHP unit directly. In this phase, the solar thermal has a higher contribution than in the heating mode, because the cooling demand occurs only in the daytime. In addition, the total share of the tank and the ASHP is lower than 6% of the total output, and especially of the proposed system when considering the energy level, or 1.8%. However, because of the priority of the WCC in the cooling mode, a higher share of cooling comes from the WCC int the modified method , or 4601 MWh which is 1021 MWh higher than in the system with conventional method, which results in the most expensive cost of chilled water, or 132.850 J/J (Table 9).

4.3 Annual performance

To analyze the annual performance of the proposed system, the exergy efficiency is used here defined as the ratio of total exergy output (containing exergy of cooling, heating, and electricity) to the total input (including exergy of natural gas, solar irradiance, and grid electricity). Together with natural gas and grid electricity consumption, the monthly exergy efficiency of the system considering the energy level is plotted in Fig. 8.

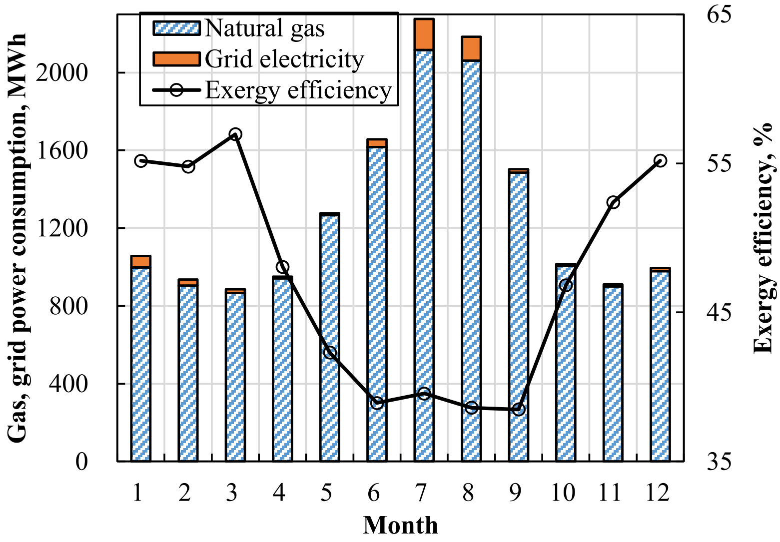

Fig. 8. Monthly natural gas and grid electricity consumption and exergy efficiency.

Owing to the lower heating demand, the gas and grid electricity consumption in the heating mode is lower, especially in March and November, while the input in the cooling mode is very high, especially in July and August. In July, the natural gas and grid power consumption is 2.4 and 8.3 times of that in March. Additionally, compared to grid electricity, the natural gas accounts for a higher contribution in the hybrid system due to the vital role of the GT. The total natural gas consumption over the whole year is 29 times higher than the grid power consumption. On the other hand, the maximum exergy efficiency of the proposed system is 57.0% in March followed by January and December with 55.2%, while the exergy efficiency in the cooling mode is < 45%, due to the higher chilled water demand at lower energy level, especially in September (38.5%).

The performance of the cooling and heating devices are essential for the overall system performance, for which reason the partial load performance of the devices is considered in the simulation, (Table A1). The hourly COP of the WCC, ASHP, and AHP are displayed in Fig. 9.

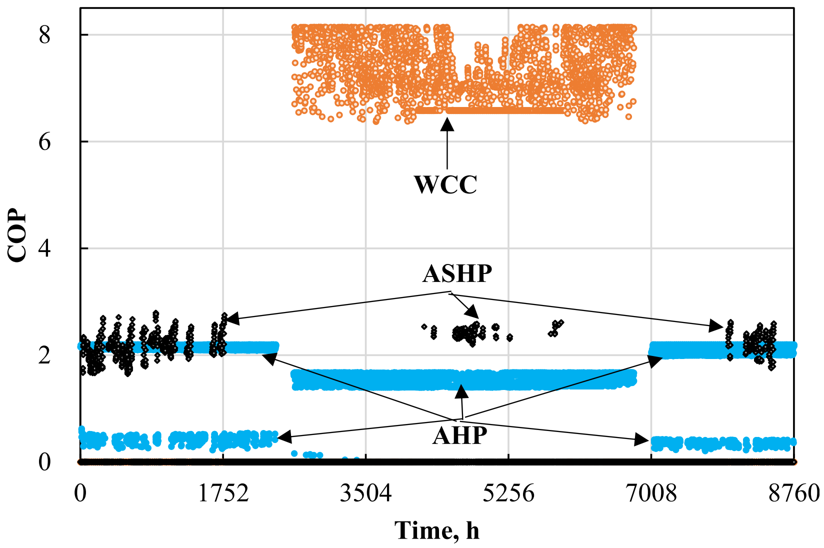

Fig. 9. Hourly COP of the WCC, ASHP, and AHP.

It can be seen from Fig. 9 that the performance of the AHP in the cooling mode is more steady than in the heating mode, because the GT works with a higher partial efficiency resulting from the higher cooling demand. The average COP of the AHP in the cooling and heating mode are 1.5, and 1.9, respectively. Compared to other two devices, the COP of the WCC is the largest with an average value of 7.2. For the ASHP-unit, it can supply heating water in the heating mode and chilled water in the cooling mode. The ASHP worked 741 hours and 112 hours in heating and cooling modes over the whole year, with an average COP of 2.1 and 2.4, respectively.

4.4 Discussion

In the simulation of the thermo-ecological cost, the STEC of the grid electricity and natural gas are two most essential parameters that influence the performance of the proposed system. In the next, the impacts of varying the STEC of the grid electricity and natural gas increases from -30% to +30% is analyzed.

(1) Effect of thermo-ecological cost of grid electricity

The impact of the STEC of grid electricity on the products are displayed in Fig. 10. With increasing STEC of grid electricity in Fig. 10(a), the corresponding STEC of electricity in heating and cooling modes and over the whole year is slightly increased. The cost increases by 0.01, 0.02, and 0.01 J/J. The influence on the cost of the heating, cooling water, and hybrid system in Fig. 10(b) is similar, increasing the STEC by 0.06, 0.09, and 0.02 J/J, respectively.

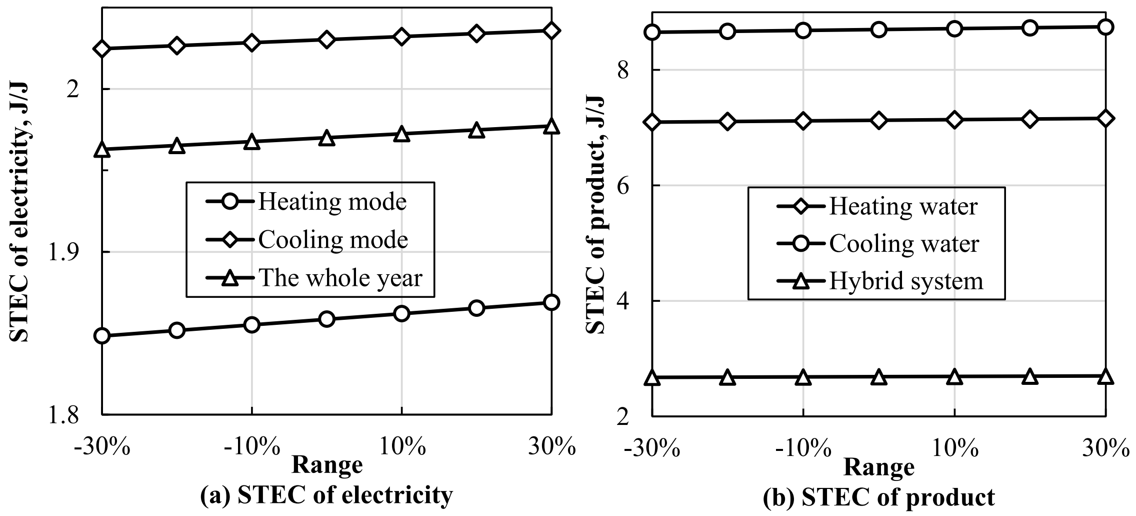

Fig. 10. Variation of the specific thermo-ecological cost with the STEC of grid electricity.

(2) Effect of thermo-ecological cost of natural gas

As Fig. 8 showed, natural gas is the main fuel in this study, and the influence of its STEC is shown in Fig. 11. The STEC of the products in Fig. 11 increases with higher STEC of natural gas. For each 10% increase in STEC in Fig. 11(a), the STEC of electricity in heating, cooling and whole year are increased by 0.16, 0.17, 0.16 J/J, and the corresponding results on the heating, chilled water, and hybrid system are 0.51, 0.69, and 0.22 J/J, respectively. Compared to the effect in Fig. 10, the STEC of the natural gas has a higher influence on the performance of hybrid system than the STEC of the electricity.

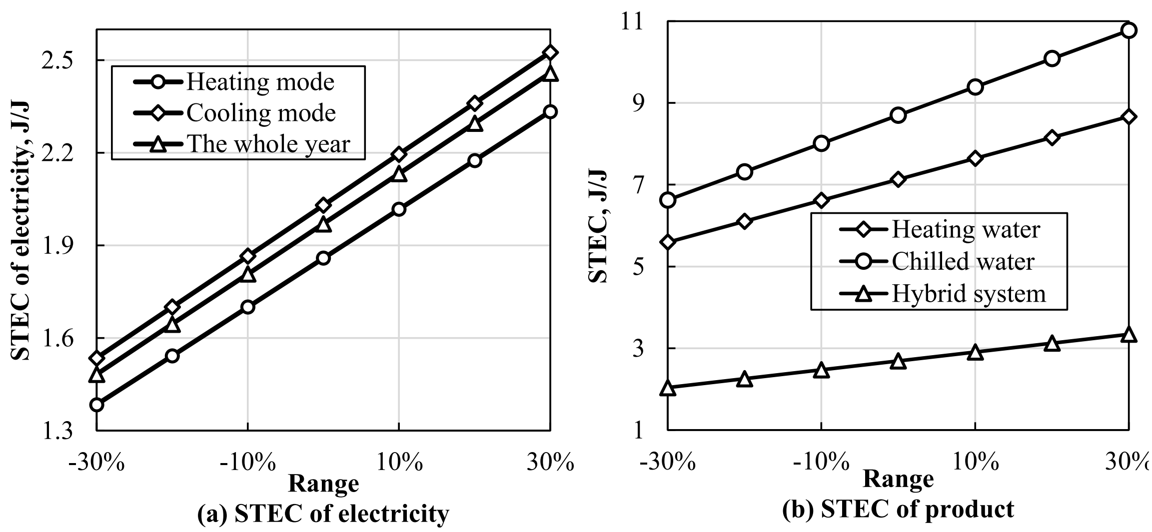

Fig. 11. Variation of the specific thermo-ecological cost with emission penalty cost.

5 Conclusions

A solar thermal and photovoltaic assisted tri-generation system is proposed in this study combining cooling, heating, and power devices, and a water-cooled chiller. An air source heat pump and water tank was used to balance the supply deficit. The thermos-ecological cost optimization from an ecological view was carried out considering the energy level of products.

Considering the energy level of the products in the so-called modified optimization method, showed that more cumulative exergy is allocated to electricity resulting in a higher specific thermo-ecological cost (STEC) of electricity, whereas the STEC of the water products is lower when using the conventional method which does not consider the energy level. The average optimized STEC of chilled and heating water decreased in this case by 1.34, and 2.93 J/J, while the STEC of electricity increased by 0.07 J/J.

The ideal area of the solar devices with the modified method is lower than the optimal values obtained with the conventional concept, whereas the other devices obtained higher capacity values, especially the water-cooled chiller. For the STEC of chilled water, the value of the water-cooled chiller was the cheapest, or 5.967 J/J, and the STEC of heating or chilled water from the tank and ASHP were the highest due to the higher wasted products in tank and the higher STEC of grid electricity, or 3.6 J/J. The water-cooled chiller was given priority to satisfy the chilled water demand - the hybrid system in the cooling mode did not produced any excess electricity, while in the heating mode, excess electricity was produced 0.25% of the total electricity demand when using the modified method and 0.43% with the conventional method.

The study shows that the water-cooled chiller is a very effective device for chilled water production reaching the highest average coefficient of performance of 7.2 among all the devices considered. The average COP of the absorption cycle was 1.9 in the heating mode and 1.5 for chilled water production, while the COP of the air source heat pump was 0.3 units higher in both modes. The STEC of the natural gas had the largest impact on the overall performance of the hybrid system due its large share in the overall consumption.

Acknowledgement

This research has been supported by the National Natural Science Foundation of China (Grant No. 22109022 and 51736006) and the Fundamental Research Funds for the Central Universities (Grant No. 2242021k30028).

Appendix

Table A1. Main energy equations of devices (Chen, Xu, Wang, Lund, & Wang, 2022).

Device	Main energy equation
GT	$\eta_{E,\mathrm{GT}}(j)=2.87\cdot \mathrm{f}_{\mathrm{GT}}^{5}(j)-9.05\cdot \mathrm{f}_{\mathrm{GT}}^{4}(j)+11.18\cdot \mathrm{f}_{\mathrm{GT}}^{3}(j)-6.99\cdot \mathrm{f}_{\mathrm{GT}}^{2}(j)+2.34\cdot \mathrm{f}_{\mathrm{GT}}(j)-0.00002$
	$\mathrm{F}_{\mathrm{NG}}^{\mathrm{GT}}(j)=E_{\mathrm{GT}}(j)/\eta_{E,\mathrm{GT}}(j)$, $Q_{\mathrm{GT}}(j)=\mathrm{F}_{\mathrm{NG}}^{\mathrm{GT}}(j)\cdot(1-\eta_{E,\mathrm{GT}}(j)-\eta_{\mathrm{loss}}^{\mathrm{GT}})$
PV	$T_{\mathrm{PV}}(j)=0.0312\cdot \mathrm{S}_{\mathrm{PV}}(j)+T_{\mathrm{a}}(j)$, $\eta_{PV}(j)=\eta_{\mathrm{PV}}^{\mathrm{std}}+\kappa\cdot(T_{\mathrm{PV}}(j)-T_{\mathrm{PV}}^{\mathrm{std}})$,
	$E_{\mathrm{PV}}(j)=\mathrm{A}_{\mathrm{PV}}\cdot \mathrm{S}_{\mathrm{PV}}(j)\cdot \eta_{\mathrm{PV}}(j)$
PTC	$\eta_{\mathrm{PTC}}=[0.7408\text{-}0.0432\cdot(\frac{T_1-T_{\mathrm{a}}}{\mathrm{S}(j)})-0.0005\cdot \mathrm{S}(j)\cdot(\frac{T_1-T_{\mathrm{a}}}{\mathrm{S}(j)})^2]\cdot 100\%$, $Q_{\mathrm{PTC}}=\eta_{\mathrm{PTC}}\cdot \mathrm{A}_{\mathrm{PTC}}\cdot \mathrm{S}\cdot 10^{-3}$
AHP	$\mathrm{COP}_{\mathrm{AHP}}^{\mathrm{c}}(j)=\frac{\mathrm{COP}_{\mathrm{std}}^{\mathrm{c}}\cdot \mathrm{f}_{\mathrm{AHP}}^{\mathrm{c}}(j)}{0.75\cdot(\mathrm{f}_{\mathrm{AHP}}^{\mathrm{c}}(j))^2+0.0195\cdot \mathrm{f}_{\mathrm{AHP}}^{\mathrm{c}}(j)+0.213}$,
	$\mathrm{COP}_{\mathrm{AHP}}^{\mathrm{h}}(j)=\frac{\mathrm{COP}_{\mathrm{std}}^{\mathrm{h}}\cdot \mathrm{f}_{\mathrm{AHP}}^{\mathrm{h}}(j)}{0.22\cdot(\mathrm{f}_{\mathrm{AHP}}^{\mathrm{h}}(j))^2+0.6698\cdot \mathrm{f}_{\mathrm{AHP}}^{\mathrm{h}}(j)+0.112}$, $\mathrm{f}_{\mathrm{AHP}}=\frac{Q_{\mathrm{AHP}}}{\mathrm{C}_{\mathrm{AHP}}}$
WCC	$\mathrm{COP}_{\mathrm{WCC}}(j)=-47.6\cdot \mathrm{f}_{\mathrm{WCC}}^{4}(j)+122.4\cdot \mathrm{f}_{\mathrm{WCC}}^{3}(j)-111.0\cdot \mathrm{f}_{\mathrm{WCC}}^{2}(j)+39.2\cdot \mathrm{f}_{\mathrm{WCC}}(j)+3.4$
Tank	$Q_{\mathrm{tk}}(j+1)=\eta_{\mathrm{tk}}\cdot Q_{\mathrm{tk}}(j)+Q_{\mathrm{tk}}^{\mathrm{ch}}(j)-Q_{\mathrm{tk}}^{\mathrm{dis}}(j)$
HE	$Q_{\mathrm{HE}}^{\mathrm{dis}}(j)=Q_{\mathrm{HE}}^{\mathrm{ch}}(j)\cdot\eta_{\mathrm{HE}}$, $\eta_{\mathrm{HE}}=90\%$
ASHP	$\mathrm{COP}_{\mathrm{ASHP}}^{\mathrm{c}}(j)=-0.052\cdot T_a+4.13$, $\mathrm{COP}_{\mathrm{ASHP}}^{\mathrm{h}}(j)=0.063\cdot T_a+2.003$

Table A2. Material consumption of units in construction stage (Chen, Xu, Wang, & Lund, 2021).

	Steel, kg/kW	Aluminum, kg/kW	Copper, kg/kW	Glass, kg/kW	PVC, kg/kW	Electricity, kWh/kW
GT	9.8	-	-	-	-	6.4
PV	27.0	10.5	-	80.0	9.2	82.0
PTC	2.5	1.1	-	0.8	4.7	5.9
AHP	18.4	-	-	-	-	11.9
ASHP	4.1	0.1	1.0	-	2.0	4.7
Tank				-		
WCC	4.1	0.04	1.1	-	2.1	4.7
HE	1.9	-	-	-	-	1.2

Table A3. Pollutant emission and electricity consumption (Chen, Hua, et al., 2022).

Item	PVC	Aluminum	Copper	Steel
SO_x, g/kg	3.4	205.5	17.7	9.7
CO_2, g/kg	247.0	25800.0	1900.0	2000.0
NO_x, g/kg	2.8	94.7	11.5	4.0
CH_4, g/kg	-	290.0	-	53.0
CO, g/kg	1.1	14.0	-	25.0
Electricity, kWh/kg	21.9	36.1	1.8	1.7

Table A4. Equivalent SO_x, CO_2, and dust emissions (Chen, Hua, et al., 2022).

Item	SO_x	CO_2	CH_4	CO	Dust
Eqv. SO_x, g/g	1.0	-	-	-	-

Eqv. CO_2, g/g	-	1.0	21.0	3.0	-
Eqv. Dust, g/g	1.9	-	-	-	1.0

Table A5. Equivalent SO_x, CO_2, and dust emissions (F. Ren, Wang, Zhu, & Chen, 2019).

Item	Data
Iteration number	300
Populations	100
Mutation probability	0.1
Distribution index of mutation operator	20
Crossover probability	0.9
Distribution index of crossover operator	20

References

Ahmadi, M. H., Ahmadi, M. A., Mehrpooya, M., & Sameti, M. (2015). Thermo-ecological analysis and optimization performance of an irreversible three-heat-source absorption heat pump. *Energy Conversion and Management, 90*, 175-183. doi:https://doi.org/10.1016/j.enconman.2014.11.021

Babaelahi, M., Rafat, E., & Mofidipour, E. (2019). Emergy-based economic and environmental analysis and multi-objective optimization of a two-cascade solar gas turbine power plant. *Sustainable Production and Consumption, 20*, 165-177. doi:https://doi.org/10.1016/j.spc.2019.06.002

Chen, Y., Hu, X., Xu, W., Xu, Q., Wang, J., & Lund, P. D. (2022). Multi-objective optimization of a solar-driven trigeneration system considering power-to-heat storage and carbon tax. *Energy, 250*, 123756. doi:https://doi.org/10.1016/j.energy.2022.123756

Chen, Y., Hua, H., Wang, J., & Lund, P. D. (2021). Thermodynamic performance analysis and modified thermo-ecological cost optimization of a hybrid district heating system considering energy levels. *Energy, 224*, 120067. doi:https://doi.org/10.1016/j.energy.2021.120067

Chen, Y., Hua, H., Xu, J., Yun, Z., Wang, J., & Lund, P. D. (2022). Techno-economic cost assessment of a combined cooling heating and power system coupled to organic Rankine cycle with life cycle method. *Energy, 239*, 121939. doi:https://doi.org/10.1016/j.energy.2021.121939

Chen, Y., Li, X., Hua, H., Lund, P. D., & Wang, J. (2022). Exergo-environmental cost optimization of a solar-based cooling and heating system considering equivalent emissions of life-cycle chain. *Energy Conversion and Management, 258*, 115534. doi:https://doi.org/10.1016/j.enconman.2022.115534

Chen, Y., Wang, J., & Lund, P. D. (2020a). Sustainability evaluation and sensitivity analysis of district heating systems coupled to geothermal and solar resources. *Energy Conversion and Management, 220*, 113084. doi:10.1016/j.enconman.2020.113084

Chen, Y., Wang, J., & Lund, P. D. (2020b). Thermodynamic performance analysis and multi-criteria optimization of a hybrid combined heat and power system coupled with geothermal energy. *Energy Conversion and Management, 210*, 112741. doi:https://doi.org/10.1016/j.enconman.2020.112741

Chen, Y., Wang, J., Ma, C., & Gao, Y. (2019). Thermo-ecological cost assessment and optimization for a hybrid combined cooling, heating and power system coupled with compound parabolic concentrated-photovoltaic thermal solar collectors. *Energy, 176*, 479-492. doi:10.1016/j.energy.2019.03.185

Chen, Y., Xu, J., Wang, J., & Lund, P. D. (2021). Exergo-environmental cost optimization of a combined cooling, heating and power system using the emergy concept and equivalent emissions as ecological boundary. *Energy, 233*, 121124. doi:https://doi.org/10.1016/j.energy.2021.121124

Chen, Y., Xu, J., Wang, J., Lund, P. D., & Wang, D. (2022). Configuration optimization and selection of a photovoltaic-gas integrated energy system considering renewable energy penetration in power grid. *Energy Conversion and Management, 254*, 115260. doi:https://doi.org/10.1016/j.enconman.2022.115260

Chen, Y., Xu, J., Zhao, D., Wang, J., & Lund, P. D. (2021). Exergo-economic assessment and sensitivity analysis of a solar-driven combined cooling, heating and power system with organic Rankine cycle and absorption heat pump. *Energy, 230*, 120717. doi:https://doi.org/10.1016/j.energy.2021.120717

Chen, Y., Xu, Z., Wang, J., Lund, P. D., Han, Y., & Cheng, T. (2022). Multi-objective optimization of an integrated energy system against energy, supply-demand matching and exergo-environmental cost over the whole life-cycle. *Energy Conversion and Management, 254*, 115203. doi:https://doi.org/10.1016/j.enconman.2021.115203

Chen, Y., Zhao, D., Xu, J., Wang, J., & Lund, P. D. (2021). Performance analysis and exergo-economic optimization of a solar-driven adjustable tri-generation system. *Energy Conversion and Management, 233*, 113873. doi:https://doi.org/10.1016/j.enconman.2021.113873

Chengjiang, Q., Mingguang, Z., Yinting, C., & Rui, W. (2014). A Quantitative Judgement Method for Safety Admittance of Facilities in Chemical Industrial Parks based on G1-Variation Coefficient Method. *Procedia Engineering, 84*, 223-232. doi:https://doi.org/10.1016/j.proeng.2014.10.429

Delač, B., Pavković, B., & Lenić, K. (2018). Design, monitoring and dynamic model development of a solar heating and cooling system. *Applied Thermal Engineering, 142*, 489-501. doi:https://doi.org/10.1016/j.applthermaleng.2018.07.052

Ebrahimi-Moghadam, A., Farzaneh-Gord, M., Jabari Moghadam, A., Abu-Hamdeh, N. H., Lasemi, M. A., Arabkoohsar, A., & Alimoradi, A. (2021). Design and multi-criteria optimisation of a trigeneration district energy system based on gas turbine, Kalina, and ejector cycles: Exergoeconomic and exergoenvironmental evaluation. *Energy Conversion and Management, 227*, 113581. doi:https://doi.org/10.1016/j.enconman.2020.113581

Egilmez, G., Kucukvar, M., & Park, Y. S. (2016). Supply chain-linked sustainability assessment of the US manufacturing: An ecosystem perspective. *Sustainable Production and Consumption, 5*, 65-81. doi:https://doi.org/10.1016/j.spc.2015.10.001

Erzen, S., Ünal, C., Açıkkalp, E., & Hepbasli, A. (2021). Sustainability analysis of a solar driven hydrogen production system using exergy, extended exergy, and thermo-ecological methods: Proposing and comparing of new indices. *Energy Conversion and Management, 236*, 114085. doi:https://doi.org/10.1016/j.enconman.2021.114085

Gładysz, P., Saari, J., & Czarnowska, L. (2020). Thermo-ecological cost analysis of cogeneration and polygeneration energy systems - Case study for thermal conversion of biomass. *Renewable Energy, 145*, 1748-1760. doi:https://doi.org/10.1016/j.renene.2019.06.088

Hasanzadeh, A., Chitsaz, A., Mojaver, P., & Ghasemi, A. (2021). Stand-alone gas turbine and hybrid MCFC and SOFC-gas turbine systems: Comparative life cycle cost, environmental, and energy assessments. *Energy Reports, 7*, 4659-4680. doi:https://doi.org/10.1016/j.egyr.2021.07.050

Jiang, K. (2019). *Application and research of oil-free centrifugal chillers in public buildings.* (Bacholar degraee). Qingdao University of Technology, Qingdao.

Kasaeian, A., Bellos, E., Shamaeizadeh, A., & Tzivanidis, C. (2020). Solar-driven polygeneration systems: Recent progress and outlook. *Applied Energy, 264*, 114764. doi:https://doi.org/10.1016/j.apenergy.2020.114764

Luo, X. J., Oyedele, L. O., Owolabi, H. A., Bilal, M., Ajayi, A. O., & Akinade, O. O. (2020). Life cycle assessment approach for renewable multi-energy system: A comprehensive analysis. *Energy Conversion and Management, 224*, 113354. doi:https://doi.org/10.1016/j.enconman.2020.113354

Madathil, D., V, R. P., Nair, M. G., Jamasb, T., & Thakur, T. (2021). Consumer-focused solar-grid net zero energy buildings: A multi-objective weighted sum optimization and application for India. *Sustainable Production and Consumption, 27*, 2101-2111. doi:https://doi.org/10.1016/j.spc.2021.05.012

Mehrabadi, Z. K., & Boyaghchi, F. A. (2021). Exergoeconomic and exergoenvironmental analyses and optimization of a new low-CO2 emission energy system based on gasification-solid oxide fuel cell to produce power and freshwater using various fuels. *Sustainable Production and Consumption, 26*, 782-804. doi:https://doi.org/10.1016/j.spc.2020.12.041

Ren, F., Wang, J., Zhu, S., & Chen, Y. (2019). Multi-objective optimization of combined cooling, heating and power system integrated with solar and geothermal energies. *Energy Conversion and Management, 197*, 111866. doi:https://doi.org/10.1016/j.enconman.2019.111866

Ren, J. (2018). Multi-criteria decision making for the prioritization of energy systems under uncertainties after life cycle sustainability assessment. *Sustainable Production and Consumption, 16*, 45-57. doi:https://doi.org/10.1016/j.spc.2018.06.005

Sajid, M. U., & Bicer, Y. (2021). Comparative life cycle cost analysis of various solar energy-based integrated systems for self-sufficient greenhouses. *Sustainable Production and Consumption, 27*, 141-156. doi:https://doi.org/10.1016/j.spc.2020.10.025

Stanek, W., & Czarnowska, L. (2018). Thermo-ecological cost – Szargut's proposal on exergy and ecology connection. *Energy, 165*, 1050-1059. doi:https://doi.org/10.1016/j.energy.2018.10.040

Stanek, W., Czarnowska, L., Gazda, W., & Simla, T. (2018). Thermo-ecological cost of electricity from renewable energy sources. *Renewable Energy, 115*, 87-96. doi:https://doi.org/10.1016/j.renene.2017.07.074

Stanek, W., Mendecka, B., Lombardi, L., & Simla, T. (2018). Environmental assessment of wind turbine systems based on thermo-ecological cost. *Energy, 160*, 341-348. doi:https://doi.org/10.1016/j.energy.2018.07.032

Stanek, W., Simla, T., & Gazda, W. (2019). Exergetic and thermo-ecological assessment of heat pump supported by electricity from renewable sources. *Renewable Energy, 131*, 404-412. doi:https://doi.org/10.1016/j.renene.2018.07.084

Stanek, W., Simla, T., Rutczyk, B., Kabaj, A., Buliński, Z., Szczygieł, I., . . . Gładysz, P. (2019). Thermo-ecological assessment of Stirling engine with regenerator fed with cryogenic exergy of liquid natural gas (LNG). *Energy, 185*, 1045-1053. doi:https://doi.org/10.1016/j.energy.2019.07.116

Szargut, J. (1987). Analysis of cumulative exergy consumption. *International Journal of Energy Research, 11*(4), 541-547. doi:https://doi.org/10.1002/er.4440110410

Venettacci, S., Cozzolino, R., Ponticelli, G. S., & Guarino, S. (2022). Environmental and economic life cycle assessment of thermal energy storage based on organic phase change material embedded in open-cell copper foams. *Sustainable Production and Consumption, 29*, 387-405. doi:https://doi.org/10.1016/j.spc.2021.10.026

Wang, J., Han, Z., & Guan, Z. (2020). Hybrid solar-assisted combined cooling, heating, and power systems: A review. *Renewable and Sustainable Energy Reviews, 133*, 110256. doi:https://doi.org/10.1016/j.rser.2020.110256

Wang, J., Lu, Z., Li, M., Lior, N., & Li, W. (2019). Energy, exergy, exergoeconomic and environmental (4E) analysis of a distributed generation solar-assisted CCHP (combined cooling, heating and power) gas turbine system. *Energy, 175*, 1246-1258. doi:https://doi.org/10.1016/j.energy.2019.03.147

Wang, J., Yang, Y., Mao, T., Sui, J., & Jin, H. (2015). Life cycle assessment (LCA) optimization of solar-assisted hybrid CCHP system. *Applied Energy, 146*, 38-52. doi:https://doi.org/10.1016/j.apenergy.2015.02.056

Wang, J., Zhou, Y., Zhang, X., Ma, Z., Gao, Y., Liu, B., & Qin, Y. (2021). Robust multi-objective optimization with life cycle assessment of hybrid solar combined cooling, heating and power system. *Energy Conversion and Management, 232*, 113868. doi:https://doi.org/10.1016/j.enconman.2021.113868

Wu, D., Zuo, J., Liu, Z., Han, Z., Zhang, Y., Wang, Q., & Li, P. (2019). Thermodynamic analyses and optimization of a novel CCHP system integrated organic Rankine cycle and solar thermal utilization. *Energy Conversion and Management, 196*, 453-466. doi:https://doi.org/10.1016/j.enconman.2019.06.020

Xu, J., Chen, Y., Wang, J., Lund, P. D., & Wang, D. (2022). Ideal scheme selection of an integrated conventional and renewable energy system combining multi-objective optimization and matching performance analysis. *Energy Conversion and Management, 251*, 114989. doi:https://doi.org/10.1016/j.enconman.2021.114989

Yuan, X., Liu, Y., & Bucknall, R. (2021). Optimised MOPSO with the grey relationship analysis for the multi-criteria objective energy dispatch of a novel SOFC-solar hybrid CCHP residential system in the UK. *Energy Conversion and Management, 243*, 114406. doi:https://doi.org/10.1016/j.enconman.2021.114406